

Transition metal-promoted oxidation catalysis by fluorite oxides: A study of CO oxidation over Cu–CeO₂

Wei Liu^{a,1}, Maria Flytzani-Stephanopoulos^b

^a Department of Chemical Engineering, Massachusetts Institute of Technology, Cambridge, MA 02139, USA

^b Department of Chemical Engineering, Tufts University, Medford, MA 02155, USA

Abstract

In this paper, the Cu–CeO₂ system is chosen as a model catalyst and CO oxidation is used as a probe reaction to illustrate the strong interaction and synergism observed when transition metal-promoted fluorite oxides are used as total oxidation catalysts. It was found that only small amounts of copper are sufficient to promote the catalytic activity of CeO₂ by several orders of magnitude, while excessive amounts of copper (Cu/(Cu + Ce) > 0.05) are detrimental to the catalyst thermal and hydrothermal stability. Heating the catalyst to temperatures over 800 °C has a significant impact on the catalytic activity because of crystal growth of cerium oxide, loss of surface oxygen, and copper aggregation.

Keywords: Oxygen mobility; Synergism; CO oxidation; Cu–CeO₂ catalyst; Thermal stability; Strong interaction

1. Introduction

Oxygen mobility is an important property of transition metal oxide catalysts used for hydrocarbon oxidation [1–3]. Oxygen species on an oxide catalyst include various types of adsorbed oxygen and lattice oxygen. In general, the former is considered important for complete oxidation or combustion, while the latter contributes to selective oxidation. Many studies of the correlation of oxygen mobility with catalytic activity have been reported in the literature. Although there has never been a clear definition, oxygen mobility can be characterized by oxygen adsorption/desorption rate and capacity, surface oxygen exchange rate with gaseous oxygen, and mobility of oxygen on and in the catalyst. Fluorite oxides, commonly comprising CeO₂, ZrO₂, HfO₂, and ThO₂, are known for their high oxygen mobility and high oxygen vacancy properties and are well studied as oxygen ion conducting materials [4,5]. From this point of view, the fluorite oxides are appropriate candidates as oxidation catalyst components. These materials are superior to the conventional transition metal oxidation catalysts such as V₂O₅, CuO, Co₃O₄, etc., in chemical and physical stability. The fluorite oxides have a cubic crystal structure over a wide temperature range. In addition, alkaline earth and rare earth oxides have substantial solubility in the fluorite oxide [6] and can be used

to modify structural and chemical properties of the fluorite oxide.

Fluorite oxides neat or mixed with other metal oxides are active catalysts for the oxidative coupling of methane at high reaction temperatures [7]. However, the fluorite oxides have traditionally not been considered as active oxidation catalysts at moderate reaction temperatures. They are mainly used as catalyst additives. Notably, CeO₂ has been widely used in the three-way automotive catalytic converter as a thermal stabilizer and oxygen storage medium [8]. But, recent research on the precious metals (Rh, Pt)/CeO₂ system has revealed that, in addition to the above-mentioned functions, cerium oxide can alter the catalytic activity of precious metal catalysts and exhibit a synergistic effect [8–13]. The synergism represents an enhanced and unique catalytic property beyond a simple additive result when two different kinds of materials are combined, such as, in the Cu/ZnO system for the hydrogenation of CO to methanol and the water–gas–shift (WGS) reaction [14], and in the (Cu, Ag, Au)/ZrO₂ system for hydrogenation of CO₂ [15]. Theories about the synergism in catalysis are still in infancy. For metal/oxide catalysts, a junction effect explanation has been proposed [16].

Along the lines of oxygen mobility and synergism, we recently proposed the transition metal modified-fluorite oxides of the form



¹ Current address: Mail Station H-2, Amoco Research Center, P.O. Box 3011, Naperville, IL 60566, USA.

as a general oxidation catalyst [17]. In the above catalyst formula, FO_2 is a fluorite oxide, DO_8 represents a dopant oxide consisting of alkaline earth and rare earth oxides, and M is an active transition metal catalyst (e.g. Cu, Co, Mn, etc.). The basic idea is that the transition metals are used in minor amounts to promote the catalytic activity of the fluorite oxide, while the fluorite oxide comprises the major catalyst component and backbone of the catalyst structure. Our previous studies showed that this catalyst system is active for SO_2 reduction by CO to elemental sulfur [18,19] and total oxidation of CO and methane [20,21]. A remarkable synergism was demonstrated through these reactions.

In the present study we focused on CO oxidation over the Cu–CeO₂ catalyst to further elucidate the oxidation properties and synergistic mechanism of the catalyst system. We examined both the effect of thermal treatment on the catalyst activity and the effect of catalyst composition on the catalyst thermal stability. Furthermore, we prepared and studied mixed oxide catalysts of nano CuO (very fine powder) and CeO₂. The structural simplicity of this catalyst enabled us to obtain unambiguous information about Cu–CeO₂ interaction and activity enhancement.

2. Experimental

Bulk composite Cu–Ce–O catalysts were prepared by coprecipitating aqueous salt solutions of the metals with ammonium carbonate or sodium carbonate. Cerium in the catalyst formula is designated as Ce(La) when the cerium nitrate precursor used in the preparation contained 1.5 wt.% La (99% purity, Aldrich). The catalysts were calcined in air at 650 °C for 4 h. More details on the preparation can be found elsewhere [17,20]. Bulk CuO and CeO₂ were prepared by thermal decomposition, respectively, of copper carbonate at 650 °C and cerium acetate (99.9%) at 750 °C for 4 h. The resulting CeO₂ had a crystal size of ca. 17 nm, an average pore size of ca. 20 nm, and BET surface area of ca. 28 m² g⁻¹, while the bulk CuO had a crystal size of ca. 100 nm and BET surface area of 1.8 m² g⁻¹. Very fine CuO powder, nano-CuO, was specially synthesized in an ultrahigh vacuum (UHV) apparatus by magnetron sputtering without air calcination [22]. The crystallinity of the nano-CuO could not be detected by X-ray diffraction and its particle size was estimated to be ca. 2 nm by high-resolution transmission electron microscope. The nano-CuO + CeO₂ mixture was prepared by mixing the nano-CuO powder, CeO₂ powder, and de-ionized water for 10 min in an ultrasonic water bath at room temperature. The amount of water used was just enough to cover the powder. The well mixed slurry was then dried in air at 300 °C for 1 h.

The catalyst crystal phase composition was analyzed by X-ray powder diffraction (XRD) on a Rigaku 300 X-ray Diffractometer. Copper $K\alpha_1$ radiation was used with power setting of 50 kV and 200 mA. Typical operation parameters were a divergence slit of 1°, scattering slit of 1°, receiving slit

of 0.15°, and scan rate of 1 to 10° min⁻¹ with a 0.02° data interval. The catalyst morphology was observed with scanning electron microscopy (SEM) on a Cambridge Stereoscan 240 MK.3 instrument. The catalyst microstructure was studied by a state-of-the-art Vacuum Generators HB603 scanning transmission electron microscope (STEM) equipped with an X-ray microprobe of 0.14 nm optimum resolution. For STEM analysis, the catalyst powder was dispersed on a nickel grid coated with a carbon film. The elemental mapping was conducted with the X-ray probe on the basis of a 128 × 128 or 256 × 256 data matrix. The catalyst surface was analyzed by X-ray photoelectron spectroscopy (XPS) on a Perkin–Elmer 5100 system. For XPS analysis, the catalyst powder was mounted on a tantalum foil and placed into the vacuum chamber without any pretreatment. A magnesium X-ray source was used with power setting of 15 kV and 20 mA. The binding energy was adjusted to the C 1s peak at 284.6 eV which existed in all measurements as an impurity. Temperature programmed reduction (TPR) was performed on a Cahn 131 Thermogravimetric Analyzer (TGA) coupled with a MKS-RS mass spectrometer for gas analysis. A Dupont 951 TGA was also used for some TPR tests.

The reactor was a 0.6 cm I.D. × 50 cm long quartz tube heated by a Lindberg furnace. A HP5880A Gas Chromatograph (GC) equipped with a Thermal Conductivity Detector (TCD) was used for gas analysis. In catalyst activity tests, the catalyst loading was typically 0.15 g and the gas flow rate was set at 100 sccm, with a corresponding contact time of 0.09 s g cm⁻³ and space velocity of ~40 000 v/v h⁻¹ for the Cu–Ce–O catalyst. The activity was measured under steady-state conditions. For reaction rate measurements, the catalyst was diluted with silicon carbide in a weight ratio varied from 4 to 10 and the reactor was operated in a differential mode with the conversion not exceeding 20%.

3. Results

3.1. Catalytic properties of Cu–Ce–O composites

3.1.1. Synergism of Cu–Ce–O catalyst for CO oxidation

Fig. 1 shows light-off curves of bulk CeO₂, nano-CuO, bulk CuO, and Cu–Ce–O catalysts. The light-off over the nano-CuO catalyst was close to that over the bulk CuO at low conversions (<0.5) but leveled off very slowly with increasing temperature. This was probably caused by aggregation of nano-CuO particles at higher temperatures. The crystal sizes for bulk CuO and nano-CuO are about 100 nm and 2 nm, respectively. Thus, the light-off temperature of the CuO catalyst was not lowered by decreasing the particle size. In contrast, the combination of copper and cerium oxide substantially lowered the light-off temperature. A remarkable synergism was demonstrated for CO oxidation over the Cu–Ce–O catalyst. Our previous studies [20] have shown that the light-off curves of Cu–Ce–O catalysts under the present test conditions are not much affected by Cu content, catalyst

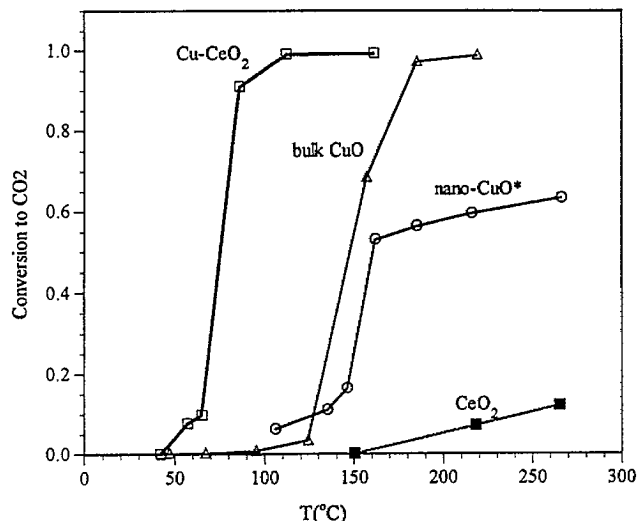


Fig. 1. CO oxidation light-off curves over CuO catalysts and the synergistic effect of the Cu–Ce–O catalyst (2% CO, 16% O₂, 0.09 sg cm⁻³; 150 mg catalyst; 100 sccm). *, 23 mg nano-CuO powder diluted by 127 mg SiC.

preparation method, catalyst BET surface area, and low level La dopant.

3.1.2. Effect of thermal treatment on the catalytic activity of Cu–Ce–O catalysts

For practical application, thermal aging is an important criterion in catalyst performance evaluation. The Cu–Ce–O catalysts tested above were prepared by air calcination at 650 °C. Fig. 2 shows the light-off curves of the Cu_{0.15}[Ce(La)]_{0.85}O_x and Cu_{0.15}Ce_{0.85}O_x catalysts after they were further heated at 850 °C for 3 h. Compared to Fig. 1, the light-off curves in Fig. 2 shifted to high temperature by ca. 100 °C. The Cu_{0.15}[Ce(La)]_{0.85}O_x catalyst heated in a reacting gas mixture of 2% CO and 1% O₂ showed a similar shift of the light-off curve to that heated in flowing air. This dramatic activity loss was not caused by the surface enrich-

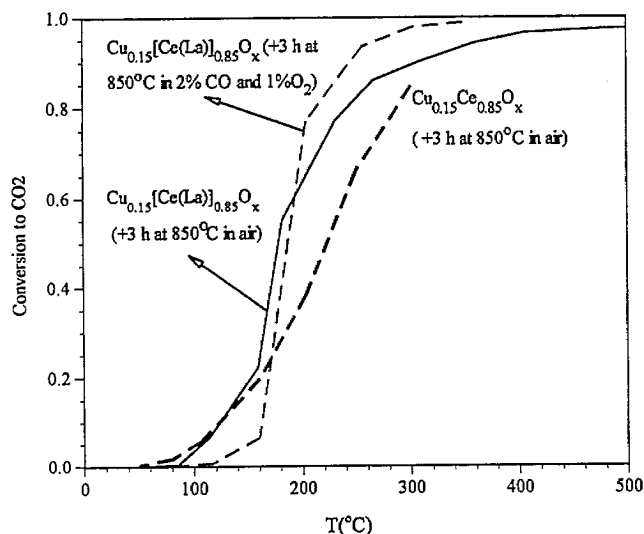


Fig. 2. Light-off curve of CO oxidation over a 15 at.% Cu–Ce–O catalyst subjected to thermal treatment (0.09 sg cm⁻³, 2% CO, 16% O₂).

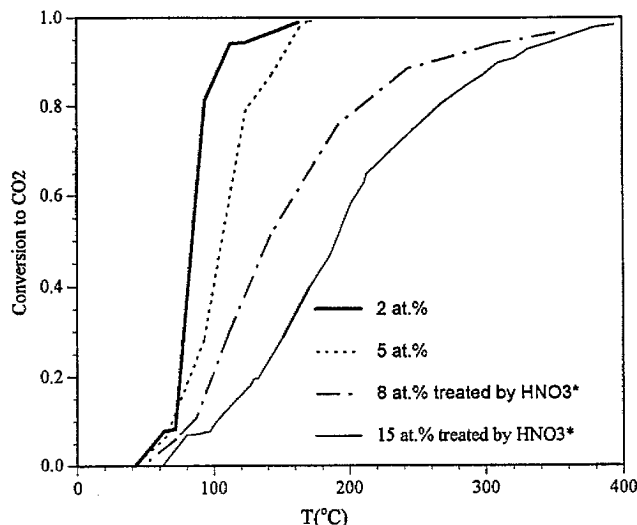


Fig. 3. CO oxidation light-off curves over Cu–Ce(La)–O catalysts prepared by 4 h air calcination at 650 °C and further heated for 3 h at 850 °C (2% CO, 16% O₂, 0.09 sg cm⁻³). *, Catalysts were treated with nitric acid prior to 850 °C heating. 6 at.% Cu and 10 at.% Cu were left in the original 8 at.% Cu and 15 at.% Cu catalysts, respectively.

ment in La, since the La-free catalyst also showed similar activity loss after heating. However, the La-doped material was superior at high conversions.

The effect of copper content in the bulk Cu–Ce–O catalyst on the thermal stability of the material is illustrated by Fig. 3. All catalysts in Fig. 3 were prepared by 4 h calcination at 650 °C and further calcined for 3 h at 850 °C, both in air. The 2 at.% catalyst had similar light-off curve to the Cu–Ce–O catalysts prepared by 650 °C calcination (Fig. 1). The light-off curve shifted to high temperatures with increasing copper content. No CuO phase was detected by XRD in the as-prepared Cu–Ce(La)–O catalyst containing 2 at.% or 5 at.% Cu. The bulk CuO phase in the as-prepared Cu–Ce(La)–O catalyst of high copper content (8 at.% and 15 at.%) was completely removed by nitric acid prior to the 850 °C heating. The treatment procedure comprised immersing the catalyst in pure HNO₃ solution for 14 h, washing it with de-ionized water, and drying it for 1 h at 650 °C. Therefore, copper can be assumed well dispersed in all these catalysts prior to high temperature heating (850 °C).

In summary, the light-off performance of Cu–Ce(La)–O can be greatly altered by heating the catalyst at 850 °C. Only catalysts of low copper content can preserve the low light-off temperature after the heating.

3.1.3. Effect of water vapor on the catalytic activity of Cu–Ce–O catalysts

The effect of water vapor on the Cu–Ce(La)–O catalyst activity after thermal treatment is illustrated by Fig. 4. A stable activity was obtained for all compositions of the Cu–Ce(La)–O catalyst prepared by 4 h calcination in air at 650 °C. However, further calcining the catalyst at 850 °C caused a loss of catalyst resistance to water vapor. The activity of the heat-treated Cu_{0.01}[Ce(La)]_{0.99}O_x seems to slowly

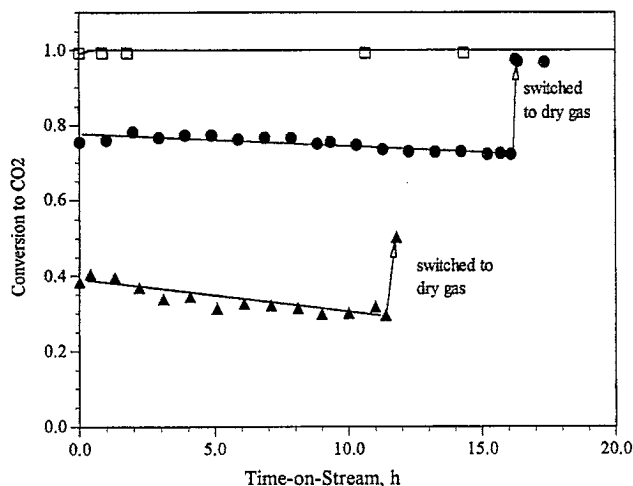


Fig. 4. Effect of water vapor on the CO oxidation activity of Cu–Ce–O catalysts (340 °C, 0.06 sg cm⁻³, 2% CO, 12% O₂, 32% H₂O). □, all Cu–Ce–O catalysts prepared by 4 h calcination in air at 650 °C; ●, Cu_{0.01}[Ce(La)]_{0.99}O_x further calcined for 3 h in air at 850 °C; ▲, Cu_{0.15}[Ce(La)]_{0.85}O_x further calcined in air at 850 °C for 3 h.

decline with time-on-stream, but immediately recovered to full conversion after the reacting gas was switched back to the dry feed gas. By contrast, the heated Cu_{0.15}[Ce(La)]_{0.85}O_x catalyst dramatically lost its activity. CO conversion over this catalyst dropped to 40% from 93% upon introduction of 32% H₂O, continued to decline with time-on-stream, and recovered to only 50% after the reacting gas was switched to dry gas. As a result, the 1 at.% containing bulk catalyst had better performance after thermal aging than the 15 at.% Cu-containing catalyst.

3.1.4. Surface properties and microstructure of thermally-aged Cu–Ce(La)–O catalysts

Fig. 5 shows the XPS analysis of 2 at.% and 15 at.% bulk catalysts after thermal aging. The copper species were identified as CuO, Cu⁺¹, and isolated Cu⁺² based on Cu 2p binding energy, Cu L₃VV Auger electron kinetic energy, catalyst microstructure, and the literature data. Comprehensive XPS data and analysis were presented in a recent publication [21]. Fig. 5 indicates that a higher fraction of the isolated copper was found on the 850 °C heated Cu_{0.15}[Ce(La)]_{0.85}O_x catalyst than on the fresh one. But, the overall Cu/(Cu+Ce+La) ratio measured by XPS for this catalyst decreased from 24% to 16% after heating because of CuO growth. The latter is accompanied by fine CeO₂ particle decoration [21], hence it becomes “invisible” to XPS.

The microstructure of the heated Cu_{0.15}[Ce(La)]_{0.85}O_x catalyst was extensively studied by STEM. Fig. 6(a)–6(c) show the typical elemental maps obtained with X-ray microprobe. In Fig. 6(a)–6(c), the upper left corner is a micrograph, the upper right corner is the O element map, the lower left corner is the Ce element map, and the lower right corner is the Cu element map. Consistent with the stronger and sharper CuO peaks found by XRD, more bulk CuO particles were observed on the 850 °C heated catalyst than on the fresh

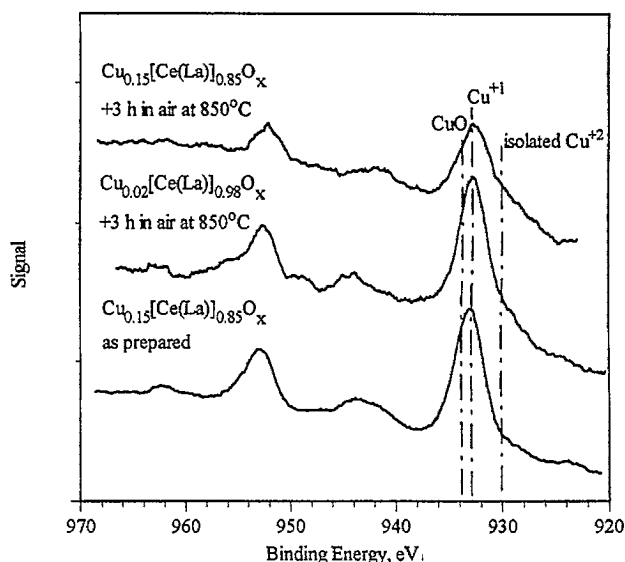


Fig. 5. Cu 2p XPS of Cu_{0.15}[Ce(La)]_{0.85}O_x and Cu_{0.02}[Ce(La)]_{0.98}O_x catalysts subjected to high temperature heating.

one. Similar to the observations with the Cu–Ce(La)–O catalyst of high copper content [21], the bulk CuO particles were associated with smaller cerium oxide particles as indicated by Fig. 6(a). However, an area mainly consisting of cerium oxide particles, such as in Fig. 6(b), shows uniform dispersion of copper in the cerium oxide matrix. The “arrow”-designated cerium oxide particle in Fig. 6(b) was analyzed by the STEM X-ray microprobe. The Cu/Ce ratios on that particle are 4.7/95.3 at the edge and 2.8/97.2 at the center. The presence of copper in this particle was confirmed, although the copper elemental map on the spot was faded due to weak contrast. Extensive dispersion of copper in the thermally-aged catalyst was more clearly revealed under high magnification, as illustrated by Fig. 6(c). The X-ray analysis of the whole area in Fig. 6(c) gave the Cu/Ce ratio as 4.8/96.2. Similarly, extensive copper dispersion was found in the Cu_{0.15}[Ce(La)]_{0.85}O_x catalyst after bulk CuO was removed by nitric acid and subsequent heating at 850 °C (Fig. 6(d)).

In summary, the STEM analyses have shown that copper distribution in the cerium oxide matrix remains after high temperature heating. Thus, the drastic activity loss cannot be explained on the basis of lower copper dispersion.

3.2. Catalytic properties of nano-CuO + CeO₂ catalysts

3.2.1. Comparison of specific activity of nano-CuO + CeO₂ and Cu–Ce–O catalysts

The composite catalyst has a complex microstructure, which makes it difficult to delineate the Cu–CeO₂ interaction and its effect on the catalytic activity. Therefore, the nano-CuO + CeO₂ catalyst is studied here due to its great simplicity. As will be discussed below, in this catalyst, fine copper clusters are dispersed only on the cerium oxide surface.

Light-off curves serve as a crude means for catalyst activity comparison. The complete activity comparison needs to be

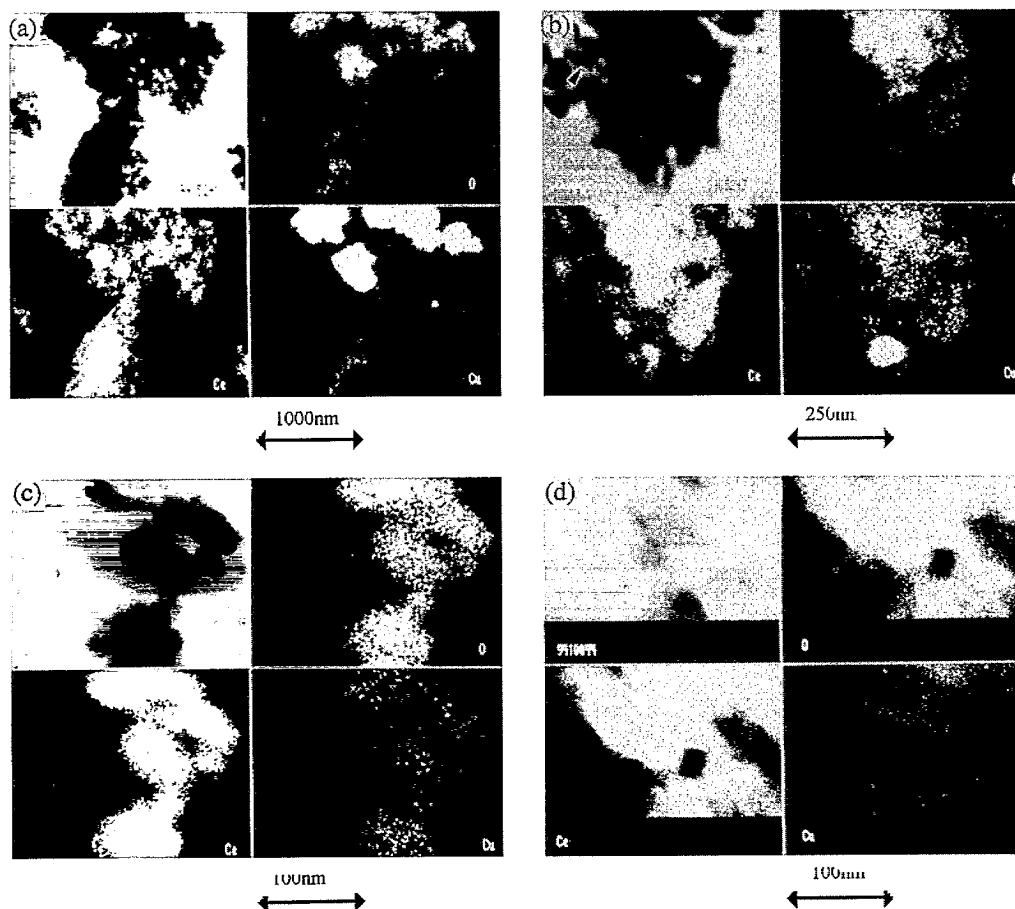


Fig. 6. STEM elemental mapping of $\text{Cu}_{0.15}[\text{Ce}(\text{La})]_{0.85}\text{O}_x$ catalyst calcined at 850°C . (a) A typical area, (b) an area of only one CuO particle, (c) an area without CuO particles, (d) a typical area of the same sample but washed by HNO_3 prior to 850°C calcination.

provided by kinetic studies. We reported in a recent paper [21] that CO oxidation kinetics over Cu–Ce–O catalysts of different bulk or surface compositions could be expressed by the following rate equation:

$$R_{\text{CO}_2} = \frac{k_{\text{CO}} K_{\text{CO}} P_{\text{CO}} P_{\text{O}_2}^n}{1 + K_{\text{CO}} P_{\text{CO}}} \quad (2)$$

Thus, a first order dependence on P_{CO} is derived if the partial pressure of CO (P_{CO}) is low enough for $K_{\text{CO}} P_{\text{CO}} < 1$. Eq. (2) is further simplified into Eq. (3) by incorporating the $k_{\text{CO}} K_{\text{CO}} P_{\text{O}_2}^n$ term into one single constant, k , because n is a small number close to zero and $P_{\text{O}_2}^n$ is nearly constant, especially when excess oxygen is present. Therefore, the apparent activation energy, E_{app} , derived from k is the difference between the intrinsic activation energy, E_a , and the heat of CO adsorption, Q .

$$R_{\text{CO}_2} = k P_{\text{CO}} \quad (3)$$

$$k = A \exp(-E_{\text{app}}/RT) \quad (4)$$

$$E_{\text{app}} = E_a - Q \quad (5)$$

Given the first order dependence at low P_{CO} , only specific rates rather than complete kinetics are reported in the following. The measurements were conducted under $P_{\text{CO}} = 0.003$

bar and $P_{\text{O}_2} = 0.003$ bar with the CO conversion not exceeding 20%. Fig. 7 shows Arrhenius plots of specific rates on the $\text{Cu}_{0.01}[\text{Ce}(\text{La})]_{0.99}\text{O}_x$ and the 25 at.% nano-CuO + CeO_2 cat-

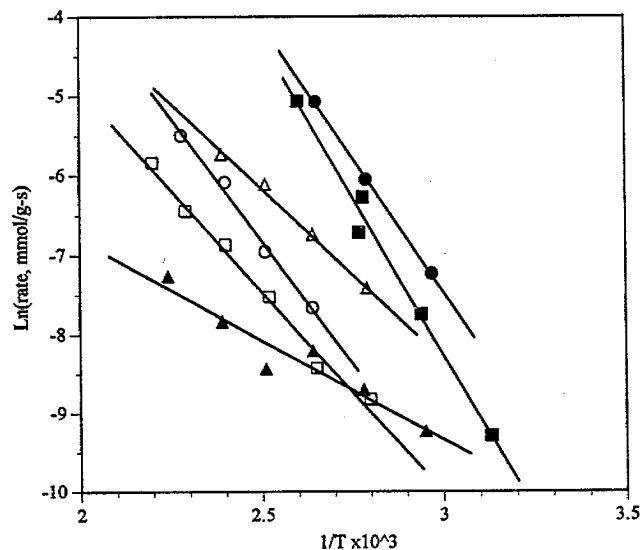


Fig. 7. Arrhenius plots of reaction rates. Filled symbols for 25 at.% nano-CuO + CeO_2 and the unfilled ones for $\text{Cu}_{0.01}[\text{Ce}(\text{La})]_{0.99}\text{O}_x$. ■ □, catalysts as-prepared; ● ○, catalysts heated for 4 h in air at 650°C ; ▲ ■, catalysts heated for 4 h at 650°C and for 3 h at 850°C , both in air.

Table 1
Effects of copper content and heating on CO oxidation rate over Cu–Ce–O catalysts

Catalyst	E_{app} (kJ mol ⁻¹)			Pre-exponential factor (mmol g ⁻¹ s ⁻¹)		
	Fresh ^b	650 °C ^c	850 °C ^d	Fresh	650 °C	850 °C
Bulk catalyst						
Cu _{0.01} [Ce(La)] _{0.99} O _x	41	51	36	1.3 × 10 ²	5.4 × 10 ³	9.3 × 10
Cu _{0.09} [Ce(La)] _{0.91} O _x	67	–	25	9.8 × 10 ⁶	–	4.2 × 10 ⁻¹
Nano-CuO + CeO ₂ mix						
2 at.% Cu ^a	58	33	15	2.4 × 10 ⁵	2.3 × 10	1.4 × 10 ⁻¹
5 at.% Cu ^a	71	83	19	4.4 × 10 ⁷	3.2 × 10 ⁹	4.3 × 10 ⁻¹
25 at.% Cu ^a	70	56	21	2.2 × 10 ⁷	3.3 × 10 ⁵	1.8 × 10 ⁻¹

^a Atomic ratio of Cu/(Cu + Ce) × 100%.

^b As-prepared.

^c Further heated for 4 h at 650 °C in flowing air.

^d Further heated for 3 h at 850 °C in flowing air following the 4 h calcination at 650 °C.

alysts subjected to thermal treatments. For the catalysts as-prepared or heated at 650 °C, the 25 at.% mixed catalyst showed about two orders of magnitude higher activity than the 1 at.% bulk catalyst, which can be rationalized in view of the higher copper content and non-linear correlation of activity with surface copper fraction [21]. After the catalyst was further heated at 850 °C, however, the 25 at.% mixed catalyst dramatically lost its activity, while the 1 at.% bulk catalyst gained significant activity.

The apparent activation energy and pre-exponential factor obtained from the Arrhenius plots are listed in Table 1 together with the data for other nano-CuO + CeO₂ mixtures and Cu_{0.09}[Ce(La)]_{0.91}O_x catalysts. Apparent activation energies for the fresh as-prepared catalysts with high copper content are similar, around 65 kJ mol⁻¹, which is higher than the values for the 1 at.% bulk and 2 at.% mixed catalysts. The pre-exponential factors for the fresh catalysts of high copper content are of the same order of magnitude, 10^{6–7}, that is 1 to 2 orders of magnitude higher than the 2 at.% Cu mixed catalyst and 4 to 5 orders of magnitude higher than the 1 at.% Cu bulk catalyst. After the catalysts were heated for 4 h in flowing air at 650 °C, the kinetic parameters (E_{app} and A) did not change much except for the 2 at.% catalyst. However, both the E_{app} and A factor were substantially decreased after the catalyst was further heated for 3 h in flowing air at 850 °C. E_{app} becomes a small number in the range of 15–36 kJ mol⁻¹, while the A factor except for the 1 at.% bulk catalyst is of the order of 10⁻¹. The A factor for the 1 at.% bulk catalyst turns out to be the greatest one. The E_{app} represents difference between the intrinsic activation energy and heat of CO adsorption. The intrinsic activation energy for CO oxidation is in the range of 73–91 kJ mol⁻¹ based on our previous results [21]. It can be approximately assumed to be a constant. Therefore, variations of E_{app} with the catalyst composition and heating treatment are attributed to the change in the heat of CO adsorption. The substantial decrease in E_{app} upon 850 °C heating results from an increased heat of CO adsorption.

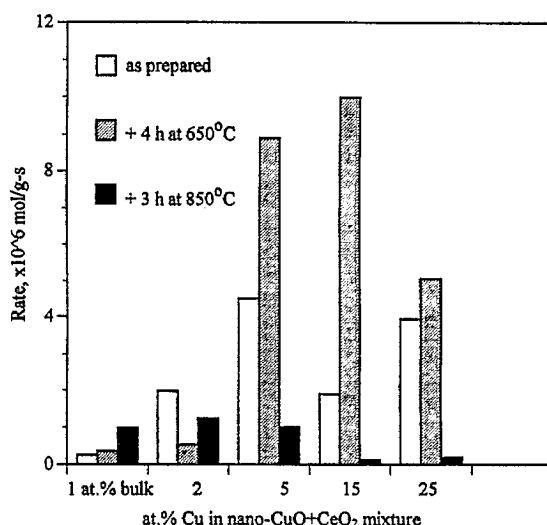


Fig. 8. Specific CO oxidation rates at 100 °C over Cu_{0.01}[Ce(La)]_{0.99}O_x and nano-CuO + CeO₂ catalysts subjected to thermal treatment.

For a clear comparison of the relative activity, specific rates measured at 100 °C for various catalysts are shown in Fig. 8. It can be seen that catalysts of high copper content have higher activity than those of low copper levels. After high temperature aging (850 °C), however, the low copper-containing catalysts showed better activity. Thus, the effect of copper content on the catalyst activity can be dramatically changed by thermal treatment. The catalyst of low copper levels again demonstrated superiority after the high temperature heating.

3.2.2. Composition and structure of the nano-CuO + CeO₂ mixture

The SEM picture in Fig. 9(a) shows that as-prepared nano-CuO looks like amorphous powder and no CuO crystals were observed, which was confirmed by XRD. The crystal size is estimated to be ca. 2 nm by high-resolution transmission electron microscopy. The STEM elemental map of the 15 at.% nano-CuO + CeO₂ in Fig. 9(b) shows that the fine copper particles or clusters were attached to the cerium oxide matrix by the mixing procedure described previously. Exten-

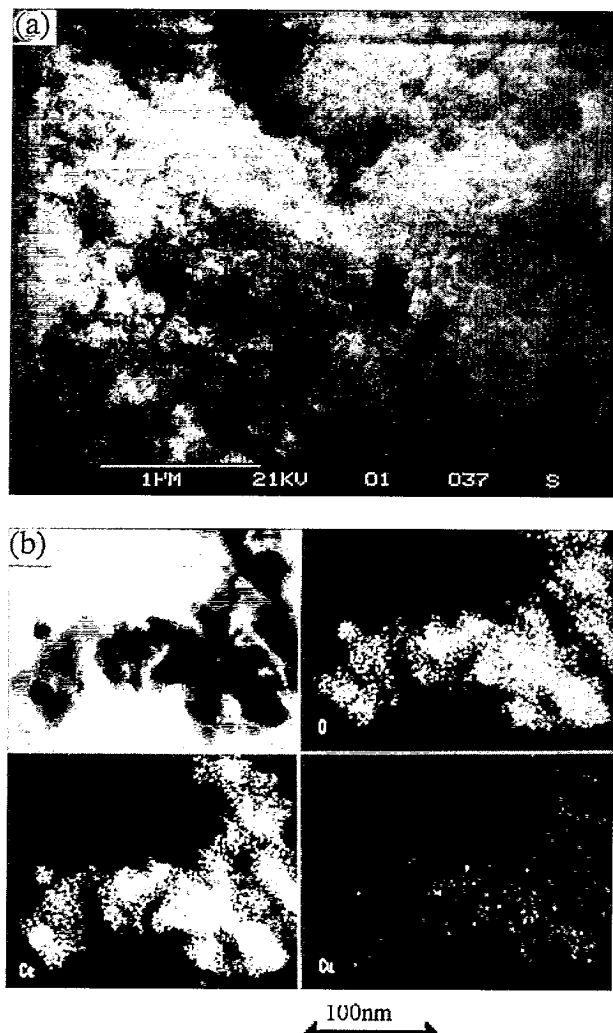


Fig. 9. (a) SEM picture of nano-CuO powder and (b) STEM elemental mapping of 15 at.% nano-CuO + CeO₂ catalyst.

sive STEM analyses revealed that the CuO clusters were well dispersed on the CeO₂ surface without any segregated large CuO particles and absence of copper in the CeO₂ bulk, which makes the nano-CuO + CeO₂ an ideal model catalyst system for studying the synergism.

Fig. 10 shows Cu 2p spectra of the nano-CuO + CeO₂ mixture. CuO and Cu⁺¹ species were identified. Different from the bulk Cu–Ce–O catalyst, the isolated copper was hardly present. Interestingly, the XPS of nano-CuO was exactly the same as that of bulk CuO. This finding is consistent with the activity measurement in Fig. 1 and confirms that reducing the CuO crystal size alone would not induce significant change of copper oxide catalytic properties. However, the Cu⁺¹ species becomes a major copper component on the nano-CuO + CeO₂ mixture of low copper content (2 and 5 at.%), while the CuO fraction is minor. A significant fraction of CuO was observed with the 25 at.% nano-CuO + CeO₂. This is not surprising because CeO₂ particles were almost covered by nano-CuO powder based on SEM observations. The Cu 2p spectra of the 5 at.% mixture after heating in air at 650 °C

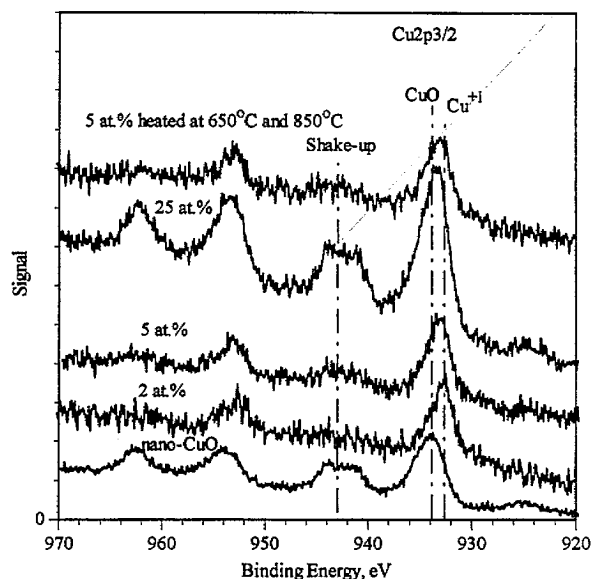


Fig. 10. Cu 2p XPS of several mixtures of nano-CuO + CeO₂ as-prepared and 5 at.% mixture heated in flowing air.

and 850 °C is similar to that of the original one. Therefore, surface copper species on this catalyst are stable.

Table 2 summarizes the XPS and XRD results. CeO₂ crystal sizes were calculated from XRD peak broadening. CeO₂ in the as-prepared nano-CuO + CeO₂ mixture has a similar size around 17 nm, because the same CeO₂ powder was used for the preparation. After the catalyst was heated in air for 4 h at 650 °C and 3 h at 850 °C, the CeO₂ crystals grew to around 44 nm size. No CuO peaks were detected in the as-prepared sample. After the catalyst was heated at high temperatures, however, broad CuO peaks of trace intensity were observed with the 5 at.% mixture while sharp and strong CuO peaks were observed with the 25 at.% mixture. The surface copper fraction as measured by XPS suggests that the copper was well dispersed in the as-prepared catalysts. Interestingly, the surface copper content for the 5 at.% catalyst increased a little after the catalyst was heated at 650 °C and 850 °C, which indicates that heating the catalyst did not drive copper into the catalyst bulk. Fig. 11 shows that the lattice spacing of CeO₂ in the nano-CuO + CeO₂ mixture did not change with copper content for either the catalysts as-prepared or the catalysts heated at 650 °C and 850 °C. These results show that nano-CuO did not form solid solution with CeO₂.

By comparing the results of the nano-CuO + CeO₂ in Tables 1 and 2, an interesting phenomenon is observed, that is, while the surface copper fraction on the 25 at.% mixture is much higher than that on the 5 at.% mixture, the pre-exponential factor *A* of the 25 at.% is less than that of the 5 at.%. Therefore, this points out that the key to high catalytic activity is to induce strong interaction of copper with cerium oxide. In the 25 at.% catalyst, most copper was not in intimate contact with cerium oxide and became redundant, while in the 5 at.% catalyst copper clusters effectively interact with CeO₂.

Table 2
CeO₂ particle sizes and XPS results of the nano-CuO + CeO₂ mixture

Catalyst	XRD results		XPS results of Cu	
	CeO ₂ crystal size (nm)	CuO peak	Major Be of Cu 2p _{3/2} (eV)	Cu/(Ce + Cu) × 100%
2 at.% Cu	16.9	no	932.8 +	13.1
5 at.% Cu	17.1	no	932.6 + 934.0	21.2
5 at.% Cu heated ^a	43.6	trace	932.6 + 934.0	24.0
25 at.% Cu	17.9	no	+ 934.0	57.8

^aHeated for 4 h at 650 °C and 3 h at 850 °C in flowing air.

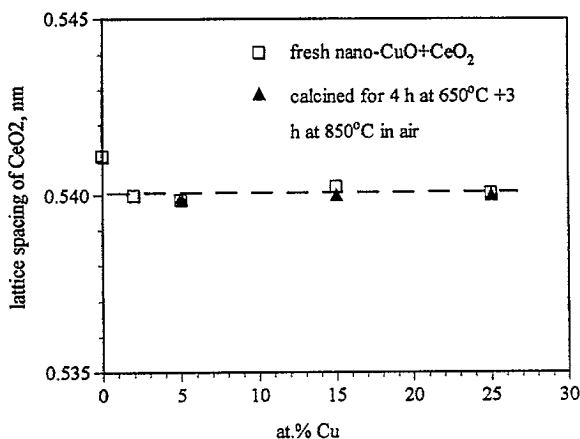


Fig. 11. Variation of CeO₂ lattice spacing with copper content and heating.

3.2.3. Temperature-programmed reduction profiles

The reducibility of a bulk Cu_{0.15}[Ce(La)]_{0.85}O_x catalyst was first investigated on a Cahn 131 TGA coupled with a MKS-RS1 mass spectrometer. The catalyst was purged for 30 min at 200 °C in 600 sccm He flow and cooled down to room temperature in He prior to the TPR run. Fig. 12 shows the reduction profiles of the catalyst in 3.5% CO/N₂ and 5% H₂/He at a temperature ramp of 10 °C min⁻¹. In CO reduction, the weight decrease was concomitant with CO₂ production. In H₂ reduction, H₂O production was difficult to be accurately detected by the MS, but, the weight decrease was

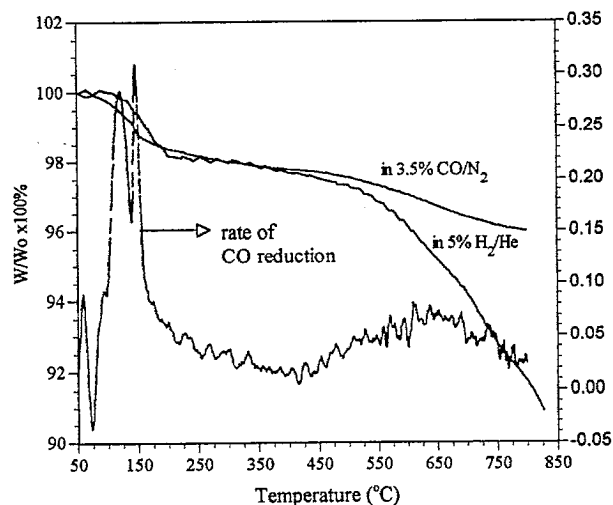


Fig. 12. TPR profiles of Cu_{0.15}[Ce(La)]_{0.85}O_x catalyst at 10 °C min⁻¹.

concomitant with H₂ decrease in the TGA outlet gas. The outlet gas compositions were not quantified, because the change in CO₂ and H₂ MS signals was small. Fig. 12 shows that the CO reduction started at ca. 80 °C and the reduction peak appeared around 120–145 °C, while the H₂ reduction occurred a little later. The weight then gradually declined. Beyond 500 °C, extensive bulk reduction began. H₂ caused much deeper reduction than CO. The bulk Cu_{0.15}[Ce(La)]_{0.85}O_x catalyst has a complex microstructure consisting of Cu ions in CeO₂ bulk, copper clusters on CeO₂ surface, and segregated CuO particles. During TPR, the surface reduction and bulk reduction took place simultaneously that the data interpretation becomes difficult. Fig. 12 shows that H₂ and CO reduction yielded different TPR profiles. To conform with most of the literature TPR studies of Cu and CeO₂ catalysts, H₂ was used in a subsequent TPR study of the nano-CuO + CeO₂ mixture.

TPR of the nano-CuO + CeO₂ mixture was performed on a Dupont 951 horizontal TGA balance. The catalyst was purged in He at 200 °C until the weight was stabilized and then, cooled down to room temperature in He. The TPR was conducted in 20% H₂/He from 50 to 850 °C at 10 °C min⁻¹. Fig. 13 shows the weight loss and reduction rate profiles of the as-prepared nano-CuO + CeO₂ catalysts. The reduction rate is calculated as follows:

$$\text{Rate} = \frac{-100 \cdot dW}{W_0 \cdot dt} \quad (6)$$

where W_0 is the initial weight and W is the sample weight at time t on stream. Two reduction peaks were found. The peak at low temperature (125 ~ 225 °C) is due to copper oxide reduction, while the peak at high temperature (600 ~ 850 °C) is due to bulk reduction of cerium oxide. The low temperature peak consists of a doublet with one peak centered at 157 °C and another centered at 180 °C. The 157 °C is a major component for 2 at.% and 5 at.% catalysts while the 180 °C is a major component for the 25 at.% catalyst. These results are consistent with the XPS data, i.e. indicate the presence of two kinds of copper (Cu⁺ and CuO). Thus, we can attribute the 157 °C peak to the copper strongly interacting with cerium oxide and the 180 °C peak to the segregated copper oxide. The reduction extent is characterized by a weight loss below 300 °C as listed in Table 3. Table 3 shows that the measured weight loss is always greater than the values calculated by

Table 3
Weight loss of the nano-CuO + CeO₂ mixture at 300 °C in TPR

Catalyst	Calculated based on CuO ^a	As-prepared		+650 °C ^b		+650 °C + 850 °C ^c
		Expt. ^d	Excess ^e	Expt. ^d	Excess ^e	Expt. ^d
2 at.% Cu	0.19%	0.59%	0.30%	–	–	0.21%
5 at.% Cu	0.48%	0.94%	0.46%	0.9%	0.42%	0.49%
25 at.% Cu	2.70%	0.32%	0.52%	–	–	2.8%

^a Weight loss calculated by assuming all Cu exists as CuO and complete reduction of CuO at 300 °C.

^b Further heated for 4 h at 650 °C in flowing air.

^c Further heated for 3 h at 850 °C in flowing air following the 4 h calcination at 650 °C.

^d Experimentally measured weight loss.

^e Difference between the measured and calculated values.

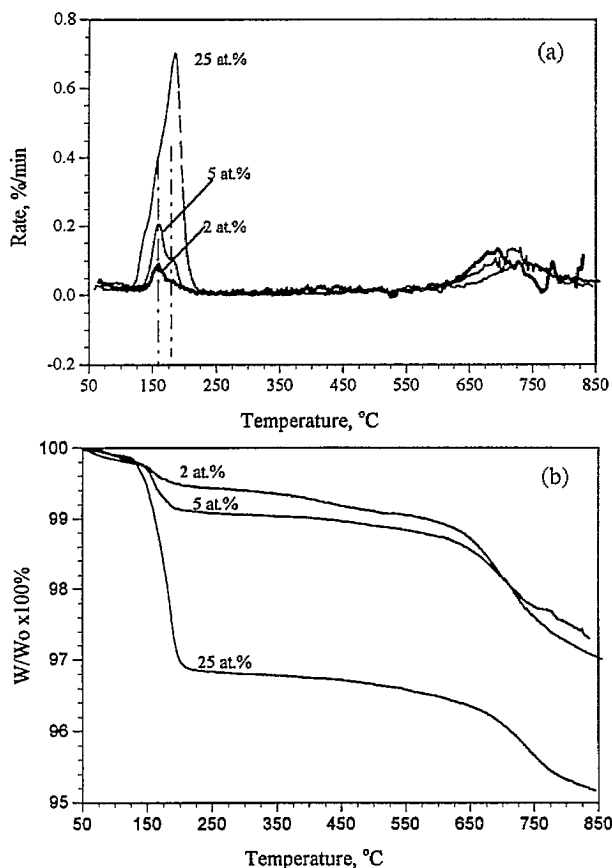


Fig. 13. TPR profiles of the as-prepared nano-CuO + CeO₂ mixtures (50 °C to 850 °C at 10 °C min⁻¹ in 20% H₂/He, pre-purged in He at 200 °C).

assuming all copper in the catalyst existing as CuO and complete reduction of CuO at 300 °C. The excess weight loss increased from 0.3% for the 2 at.% Cu catalyst to 0.52% for the 25% Cu catalyst, which corresponds to 1.6% to 2.8% reduction of cerium oxide.

TPR profiles of the heated nano-CuO + CeO₂ mixtures are shown in Fig. 14. The low temperature peak (~157 °C) was still observed with the 5 at.% Cu catalyst after 4 h calcination in air at 650 °C. Table 3 also indicates that the surface reduction extent of this catalyst is similar to the as-prepared. However, the TPR profiles were dramatically changed for all the three catalysts after 4 h calcination at 650 °C and 3 h calci-

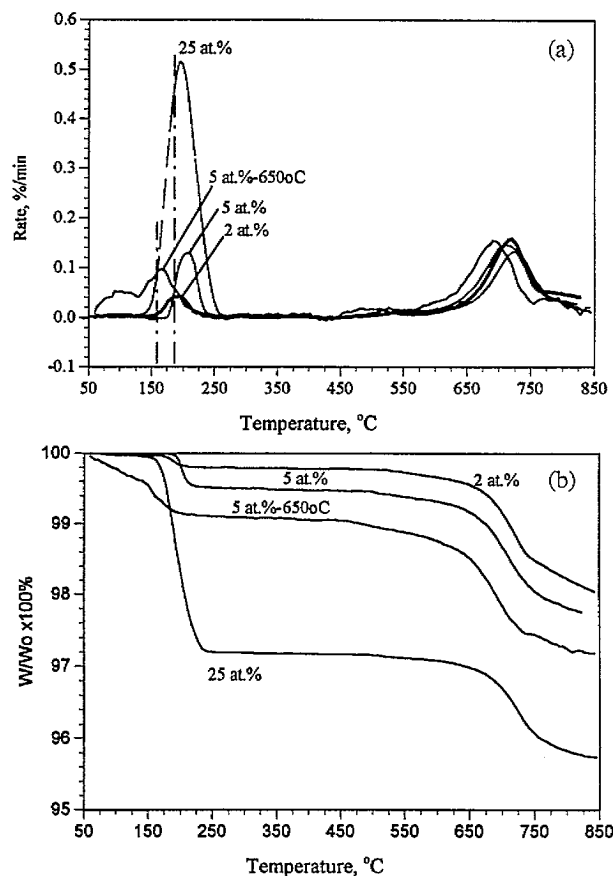


Fig. 14. TPR profiles of the nano-CuO + CeO₂ mixtures after 4 h calcination at 650 °C and 3 h calcination at 850 °C in air (50 °C to 850 °C at 10 °C min⁻¹ in 20% H₂/He).

nation at 850 °C. The doublet peak in the low temperature range was replaced with a single peak centered around 180–200 °C. This peak is considered to be due to bulk CuO reduction because large CuO particles were found in the 25 at.% Cu catalyst after the calcination. The reduction extents listed in Table 3 for these calcined samples are almost the same as the calculated values. Thus, all the weight loss below 300 °C is ascribed to CuO reduction, while surface reduction of cerium oxide is negligible for these calcined catalysts. By contrast, the rate and extent of bulk reduction (high temper-

ature peak) of the calcined catalysts are similar to those of the as-prepared catalysts.

4. Discussion

The above experimental results are explained within the framework of synergism and Cu-CeO₂ interaction model presented in a recent paper [21] and depicted in Fig. 15. Based on this model, cerium oxide provides oxygen sources, while copper clusters provide sites for CO adsorption, and the two adsorbed species react at the boundary resulting in rapid turnover of reacting species or high reaction activity. The copper clusters are stabilized by cerium oxide through an interfacial interaction and in turn promote the surface oxygen activation of cerium oxide. Cu⁺¹ species are formed through the interaction of copper clusters with cerium oxide and provide strong sites for CO adsorption. In addition, the copper clusters may keep some identity of the bulk Cu₂O material and modify the physical and chemical properties of cerium oxide through Schottky junction effects [23]. For example, Cu₂O is a p-type electronic conductor, while CeO₂ is of n-type. For an oxidation reaction involving electron transfer between the reactants and the catalyst, hybrid catalyst electronic properties may be beneficial.

The present results of the nano-CuO + CeO₂ catalysts provide supporting evidence to the synergistic model. The activity measurements in Fig. 1 show that reducing the CuO particle size did not lower the CO oxidation light-off temperature. Also, the XPS data in Fig. 10 indicate that reducing the CuO size did not alter the oxidation state of Cu. But, when the nano-CuO is put on cerium oxide as is in the nano-CuO + CeO₂ mixture, the CO oxidation activity becomes comparable to the bulk Cu-Ce-O composite catalyst which has an activity several orders of magnitude higher than the other Cu catalysts [20]. Fig. 8 shows that excessive application of nano-CuO powder on cerium oxide did not yield a higher activity, although the surface Cu fraction as measured

by XPS was indeed increased. The reason is that this excessive amount of nano-CuO had the properties of bulk CuO as shown also by TPR. Thus, only the nano-CuO particles in intimate contact with cerium oxide showed "strong interaction" and were unlike bulk CuO. The strong interaction leads to the observation of Cu⁺¹ species by XPS, lower reduction temperature in TPR, and induces surface reduction of cerium oxide.

A great amount of literature data is available for TPR studies of various Cu catalysts. A thorough study of Cu₂O, CuO, and CuO-ZnO systems was presented in a recent paper [24]. The TPR peak shape and position highly depend on the experimental conditions and the catalyst system. In this work, the H₂ reduction profile of the composite Cu-Ce-O catalyst in Fig. 12 looks different from those for the nano-CuO + CeO₂ mixture in Fig. 13. However, a reliable conclusion can be made only by comparison on the same basis. The nano-CuO + CeO₂ mixtures serve this purpose well because they were made up of the same CuO and CeO₂ powder through a simple mixing procedure. The literature data [24,25] show that the reduction peak of copper oxide typically occurs over the range of 200 to 300 °C. The TPR peak at 200 °C in Fig. 14 for the 25 at.% Cu catalyst is attributed to bulk CuO reduction, because this catalyst consisted mostly of bulk CuO after the high temperature calcination. The copper TPR peaks in Fig. 13 for the as-prepared nano-CuO + CeO₂ mixtures can be divided into two components, one at 157 °C and another at 180 °C. Taking into account the XPS and activity results, we attribute the 180 °C and the 157 °C component, respectively, to separated nano-CuO fraction and nano-CuO fraction associated with cerium oxide. The separated nano-CuO keep its identity as CuO, while the TPR profiles in Figs. 13 and 14 suggest that the reduction temperature of CuO is only slightly decreased with size as suggested by some literature [26]. The nano-CuO fraction associated with cerium oxide interacts with cerium oxide, however, is more reducible due to the strong interaction with CeO₂.

The data in Table 3 show that CuO reduction only accounts for part of the weight loss of the nano-CuO + CeO₂ mixture in the TPR run below 300 °C. Since all the samples were purged in situ by He at 200 °C prior to the TPR run, the excess weight loss is attributed to the reduction of the cerium oxide surface. The reduction extent of cerium oxide increases with the Cu at.%, because the higher the Cu content, the higher the interfacial area of copper clusters with cerium oxide. According to Ref. [9], significant reduction of CeO₂ surface occurs only at temperatures above 300 °C. But, cerium oxide surface reduction can be significantly lowered in the presence of precious metals (Pt and Pd) [9,13]. The present TPR results suggest that copper in the Cu-CeO₂ catalysts also induces the surface reduction of CeO₂ at low temperatures. Oxygen adsorption/desorption on cerium oxide have been studied extensively in the literature using various techniques [27-30]. The superoxide species (O₂⁻) is generally considered as the active surface oxygen for low temperature oxidation. Its formation is correlated with the surface reduction

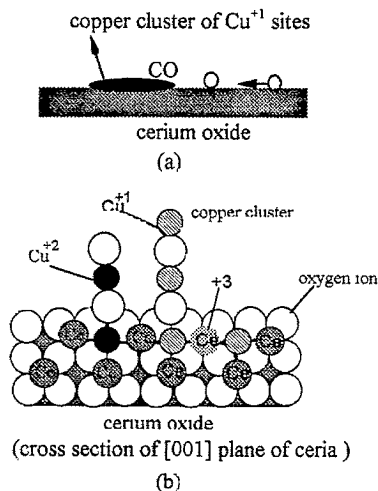


Fig. 15. Reaction and interaction models of Cu-CeO₂ catalysts. (a) synergistic reaction model, (b) strong interaction model of Cu-CeO₂.

of cerium oxide. Thus, enhancing the surface reducibility of cerium oxide promotes the generation of the active surface oxygen species.

Now we apply the synergistic model to the discussion of the effect of heating on the catalyst activity. Heating the catalyst induces growth of cerium oxide crystals and aggregation of copper clusters. The particle growths result in low catalyst surface area. But, this factor is not large enough to explain orders of magnitude loss in the activity. More importantly, cerium oxide crystal growth eliminates the surface defects and drives the copper ions out of the lattice so that Cu–CeO₂ interaction is lost and the surface oxygen is diminished. Yamada et al. [31] found that surface oxygen decreased from 224 $\mu\text{mol g}^{-1}$ for CeO₂ heated at 500 °C to only 4 $\mu\text{mol g}^{-1}$ after heating at 1 000 °C. Loss of surface oxygen of CeO₂ by high temperature heating was also reported by Lamotte et al. [32] in TPR of CeO₂ by CO. The authors found that extensive surface reduction of CeO₂ calcined at 400 °C (100 m² g⁻¹) occurred at temperatures below 500 °C, while little reduction was observed with the CeO₂ calcined at 850 °C (5 m² g⁻¹). Our TPR tests also show that the heating temperature has large effect on the surface reducibility. Heating CeO₂ at 650 °C resulted in BET surface area decrease and about proportional decline in the surface reducibility. However, heating CeO₂ at 850 °C resulted in a decrease in surface reducibility disproportionately higher than the surface area decrease. Literature information on CeO₂ crystal growth kinetics is very limited. The sintering kinetics of CeO₂ crystallite at 623 °C were studied by Pijolat et al. [33]. They found that CeO₂ can sustain a stable surface area at this temperature. A recent study of the La-doped CeO_{2-x} system [34] reported that heating at temperatures below ca. 700 °C does not cause significant crystal growth, while heating at a temperature beyond 800 °C results in substantial growth. Therefore, the catalyst heating temperature is an important factor to determine the catalyst activity. The drastic activity loss upon heating at 850 °C is, thus, attributed to cerium oxide crystal growth and the depletion of surface oxygen species.

In addition to the effect of heating on the cerium oxide crystal growth, heating also affects the interaction of copper clusters and cerium oxide. As evidenced by the data in Table 2, heating the catalyst induces significant changes to the apparent activation energy and rate constant. In the case of the 5 at.% nano-CuO + CeO₂ catalyst, ‘mild heating’, i.e. heating at 650 °C, strengthens the synergism between copper clusters and cerium oxide and thus, enhances the activity. When the factor of copper content is taken into account, the changes induced by heating are more complicated. The synergistic model suggests that only copper cluster associated with cerium oxide is the active catalyst configuration. Therefore, for the composite Cu–Ce–O catalyst of low copper content (1 at.% or 2 at.%), copper existed as isolated ions in the as-prepared state. High temperature heating drives the isolated copper to form clusters and creates an active catalyst. For the composite Cu–Ce–O catalyst of high copper content,

such as Cu_{0.15}[Ce(La)]_{0.85}O_x, a large fraction of copper already disperses on cerium oxide in the form of clusters in the as-prepared state. The high temperature heating scavenges the existing copper clusters into bulk CuO particles and the active configuration is lost. But, STEM analysis revealed that a significant portion of copper was still uniformly dispersed in the cerium oxide after the heating, probably in the form of isolated ions. It is not understood at the present time why these copper ions do not migrate onto the cerium oxide to form clusters. Perhaps, what is formed is determined by the thermodynamics of the Cu–Ce–O tertiary system. For the nano-CuO + CeO₂ mixture, only copper clusters were distributed on the cerium oxide in the as-prepared state. Copper cluster coalescence occurs upon heating. The coalescence kinetics has a second or higher order dependence to the copper cluster concentration. Therefore, the catalyst of low copper content has a slow coalescence rate and possesses a higher activity, as shown in Fig. 8 after the high temperature heating.

The kinetic measurements show that the apparent activation energies for all catalysts were substantially decreased upon 850 °C heating. This is assumed to be due to increased heat of CO adsorption. The kinetic studies of the Cu_{0.01}[Ce(La)]_{0.99}O_x catalyst [21] showed an increase of heat of CO adsorption with heating temperature. However, a better understanding of the reaction mechanism calls for a study of CO and O₂ adsorption over the Cu–CeO₂ catalyst.

5. Conclusion

The Cu–Ce–O oxide system is a very active oxidation catalyst. In this work, the CO oxidation over this catalyst system was examined in the light of the strong synergism displayed by the copper–cerium oxide interaction. Stabilization of Cu⁺¹ clusters by cerium oxide, and, in turn, increased active oxygen on the cerium oxide by the presence of copper are invoked to explain the synergism. CO adsorbs strongly on Cu⁺¹ sites and reacts with labile oxygen at the interface of the two materials. The synergistic model is strongly supported by the experimental results obtained with the nano-CuO + CeO₂ mixture. This catalyst comprised copper clusters deposited on the cerium oxide surface. Its structural simplicity was used to elucidate the observed synergism.

Heating the Cu–Ce–O catalyst induces the following processes: copper diffusion from bulk to surface, clustering of isolated copper ions, aggregation of copper clusters, strengthening copper and cerium interaction, crystal growth of cerium oxide, and decrease of active oxygen species on cerium oxide. The catalytic activity is determined by the sum of these effects. Formation of copper clusters and strong interaction of copper with cerium oxide are desirable to achieve high activity. Catalyst composition and heating temperature are two key factors to control these processes. For a catalyst prepared or calcined at temperatures around or below 650 °C, its specific reaction rate increases with copper content to a certain level (i.e. 15 at.%). For a catalyst prepared or calcined

at temperatures around or above 850 °C, a small amount of copper (e.g. < 5 at.%) is preferred, because large amounts of copper have a detrimental effect on catalytic activity. Heating the catalyst at 850 °C significantly decreased the apparent activation energy and pre-exponential factor of the rate constant. But, the decrease in the activation energy for the catalyst of high copper levels was not sufficient to compensate the decrease of the pre-exponential factor. This makes the overall specific rate lower. Rapid growth of CeO₂ crystal and depletion of surface oxygen on cerium oxide at such high temperatures are considered to be the major causes of the activity loss.

Acknowledgements

This work was supported by the US Department of Energy, University Coal research Program, under Grant DE-FG22-92PC92534. The authors would like to thank Dr. A. Tschöpe and Prof. J.Y. Ying at MIT for the synthesis of nano CuO powder and Mr. C. Wadia for his assistance in the TGA study. This work made use of the MRSEC Shared Facilities supported by the National Science Foundation under Award DMR-P400334.

References

- [1] C.N. Satterfield, *Heterogeneous Catalysis in Industrial Practice*, 2nd edn., McGraw-Hill, New York, 1991.
- [2] M. Iwamoto, Y. Yoda, N. Yamazoe and T. Seiyama, *J. Phys. Chem.*, **82** (1978) 2564.
- [3] J.J. Spivey, *Ind. Eng. Chem. Res.*, **26** (1987) 2065-2180.
- [4] P. Hagenmuller and W. Van Gool, *Solid Electrolytes*, Academic Press, New York, 1978.
- [5] H.L. Tuller and P.K. Moon, *Mater. Sci. Eng. B1*, **20** (1988) 171.
- [6] D.J. Kim, *J. Am. Ceram. Soc.*, **72** (8) (1989) 1415.
- [7] A.M. Maitra, *Appl. Catal. A: General.*, **104** (1993) 11.
- [8] A. Crucq (ed.), *Catalysis and Automotive Pollution Control II*, Elsevier Science Publishers B.V., Amsterdam, 1991.
- [9] H.C. Yao and Y.F.Y. Yao, *J. Catal.*, **86** (1984) 254-265.
- [10] S.E. Golunski, H.A. Hatcher, R.R. Rajaram and T. Truex, *Appl. Catal. B: Environ.*, **5** (1995) 367.
- [11] A.K. Datye, D.S. Kalakkad, M.H. Yao and D.J. Smith, *J. Catal.*, **155** (1995) 148.
- [12] C. Hardacre, R.M. Ormerod and R.M. Lambert, *J. Phys. Chem.*, **98** (1994) 10901.
- [13] J.G. Nunan, R.G. Silver and S.A. Bradley, in R.G. Silver, J.E. Sawyer and J.C. Summers (eds.), *Catalytic Control of Air Pollution*, ACS Symposium Series 495, American Chemical Society, Washington, DC, 1992, Chapter 17.
- [14] H. Kung, *Transition Metal Oxide: Surface Chemistry and Catalysis*, in B. Delmon and J.T. Yates (eds.), *Studies in Surface Science and Catalysis*, Vol. 45, Elsevier, Amsterdam, 1989, p. 245.
- [15] M.K. Baiker, M. Maciejewski, S. Menzi and A. Wokaun, in L. Guzzi, F. Solymosi and P. Tetenyi (eds.), *New Frontiers in Catalysis, Proc. of the 10th Int. Congress on Catalysis, Budapest, July, 1992*, Elsevier, Amsterdam, 1993, p. 1257.
- [16] J.C. Frost, *Nature*, **334** (1988) 577.
- [17] W. Liu, *Doctorate Thesis*, Massachusetts Institute of Technology, 1995.
- [18] M. Flytzani-Stephanopoulos and W. Liu, *US Patent No. 5 384 301*, 1995.
- [19] W. Liu, A.F. Sarofim and M. Flytzani-Stephanopoulos, *Appl. Catal. B: Environ.*, **4** (1994) 167-186.
- [20] W. Liu and M. Flytzani-Stephanopoulos, *J. Catal.*, **153** (1995) 304-316.
- [21] W. Liu and M. Flytzani-Stephanopoulos, *J. Catal.*, **153** (1995) 317-332.
- [22] A. Tschöpe and J.Y. Ying, *J. Nanostr. Mater.*, **4** (5) (1994) 617.
- [23] S.M. Sze, *Physics of Semiconductor Devices*, 2nd edn., Wiley, New York, 1981.
- [24] G. Fierro, M.L. Jacono, M. Inversi, P. Porta, R. Lavecchia and F. Cioci, *J. Catal.*, **148** (1994) 709.
- [25] A. L. Boyce, S. R. Graville, P.A. Sermon and M.S.W. Vong, *React. Kinet. Catal. Lett.*, **434** (1991) 1-18.
- [26] M.C. Marion, E. Garbowki and M. Primet, *J. Chem. Soc. Faraday Trans.*, **87** (1991) 1795.
- [27] C. Li, K. Domen, K.I. Maruya and T. Onishi, *J. Am. Chem. Soc.*, **111** (1989) 7683.
- [28] C. Li, K. Domen, K.I. Maruya and T. Onishi, *J. Catal.*, **123** (1990) 436.
- [29] X. Zhang and K.J. Klabunde, *Inorg. Chem.*, **31** (1992) 1706.
- [30] A.L. Tarasov, L.K. Przhival'skaya, V.A. Shvets and V.B. Kazanskii, *Kinet. Katal.*, **29** (1988) 1181.
- [31] T. Yamada, K. Kayano and M. Funabiki, in T. Inui, K. Fujimoto, T. Vchijima and M. Masono (eds.), *New Aspects of Spillover Effect in Catalysis, Proc. of the 3rd Int. Conference on Spillover, Kyoto, Japan, August, 1993*, Elsevier, Amsterdam, 1993.
- [32] A.B.J. Lamotte, J.C. Lavalley, A. Laachir, V. Perrichon, O. Touret, G.N. Sauvion, and E. Quemere, *Eur. J. Solid State Inorg. Chem.*, **28** (1991) 445.
- [33] M. Pijolat, M. Prin, M. Soustelle, O. Touret and P. Nortier, *Solid State Ionics*, **63-65** (1993) 781.
- [34] A. Tschöpe, W. Liu, M. Flytzani-Stephanopoulos and J.Y. Ying, *J. Catal.*, **157** (1995) 42.